# Transport Across a Turbulent Air-Water Interface

**C. N. S. Law and B. C. Khoo**
Dept. of Mechanical Engineering, National University of Singapore, Singapore 119260

*Turbulence structure in the immediate vicinity of the air–water interface has a dominant influence on the mass transfer across it. In this work, investigations on near-surface turbulence and mass-transfer rate were carried out for two distinct flow conditions: one with turbulence generated from beneath the interface, the other via wind shear from above the interface. Turbulence measurement with respect to the fluctuating interface was performed and Hanratty's β, the gradient of the linear variation of vertical velocity at the interface, was quantified. It is found that incorporating a near-surface turbulence parameter such as β provides a reasonable model for interfacial mass transfer, applicable to the two vastly different flow conditions studied.*

## Introduction

The turbulence structure in the immediate vicinity of the air–water interface can be considered to be an important governing parameter for the scalar transport across the surface. Many investigators have proposed models and theories to predict the heat/species transport rate across the air–water interface. Theofanous (1984), in a review of various conceptual theories, identified two major classes of models. One is the "eddy diffusivity" approach, with emphasis on the identification and quantification of "film-thickness" ($\delta$) residing right next to the interface, which is believed to govern the mass-transfer across the air–water interface. This model has the form

$$K_L \propto D/\delta \tag{1}$$

where $K_L$ is the mass-transfer velocity and $D$ is the diffusivity of the gas specimen in the liquid. The other class is the "eddy-structure" model, where the average "surface renewal" time ($\tau$) is thought to govern the interfacial mass transfer. This model has the form

$$K_L \propto \sqrt{D/\tau} \tag{2}$$

The eddy-structure or surface-renewal class produces a model that uses various velocity and length scales to approximate the renewal time. These include the popularly known large-eddies ($\tau \approx \Lambda/u'$) model and the small-eddies or turbulent-dissipation ($\tau \approx (\nu/\epsilon)^{1/2}$) model. Another approach is to quantify renewal time directly by correlating it with the observed "burst" occurrence frequency (Komori et al., 1993; Rashidi et al., 1991).

Still many other models have been proposed. Invariably, most of these models employed parameters that depend somehow on the means of turbulence generation and/or relate to the turbulence characteristic in the bulk region away from the immediate region next to the interface. It is thought that a general and robust model, capable of predicting the transport rate over different flow conditions and independent of the particular means of turbulence generation, should be based on the turbulence structure at the very vicinity of the interface. Hanratty (1990), in a review of various works that started with Sikar and Hanratty (1970), further developed by Campbell and Hanratty (1982), and culminating with McCready et al. (1986), highlighted the development of a model that relates mass transfer directly to near-surface turbulence without resorting to the conceptual model. Hanratty and coworkers noted that the characteristic thickness of the concentration boundary layer at the interface is indeed very thin. They suggested that the most dominant velocity component affecting the variation of concentration is $v$. Here, $v$ is the fluctuating velocity component in the $y$ direction, where $y$ is the distance measured (perpendicularly) from the interface. Since the concentration boundary layer is thin, derivatives in the $y$-direction are much larger than in the other directions. Therefore, the boundary-layer equation for concentration ($C$) in a turbulent flow field near a free surface can be simplified

Correspondence concerning this article should be addressed to B. C. Khoo.

as

$$\frac{\partial C}{\partial t} + v\frac{\partial C}{\partial y} = D\frac{\partial^2 C}{\partial y^2} \tag{3}$$

Hanratty further deduced that close to a mobile free surface

$$v = \beta y \tag{4}$$

That is, at the vicinity of the interface, $v$ varies linearly with $y$ with a gradient $\beta$. From the concentration boundary layer equation, it becomes apparent that $\beta$ (defined as the vertical velocity gradient at the interface) is the critical parameter that governs the interfacial mass transport. Quantification of $\beta$, or for that matter, any hydrodynamic quantities very close to the interface, is extremely difficult. Because the turbulent interface is constantly fluctuating, the measurement of $\beta$ calls for a technique that can *simultaneously* track the fluctuating interface and the flow field just beneath it. Gulliver and Tamburrino (1995) measured $\beta$ in the flow field under a moving belt where the free surface was close to being horizontal and interface tracking was unnecessary. However, in most free-surface turbulence, the interface is not flat and can move rather violently, unlike a flat solid wall. Despite the absence of any reliable data on $\beta$, McCready et al. hypothesized a statistical functional form to describe the behavior of $\beta$ and use it to numerically simulate the transport across a mobile interface. The computed mass-transfer rate results compared reasonably well to measured data of gas absorption by a liquid film, in terms of predicted trends. The preceding belies the critical importance of $\beta$ in interfacial mass transfer.

In the absence of the ability to quantify $\beta$ directly, Jahne et al. (1987) and Duke et al. (1995) proposed the use of surface-wave slope, which serves as proxy to the vertical velocity just beneath the interface. Experimental techniques for the measurement of the surface-wave slope were developed (Zhang and Cox, 1994), and the measured wave slope appears to be well correlated with measured interfacial mass-transfer rate (Saylor and Handler, 1997; Duke et al., 1995). Even then, such studies were only carried out for wind-induced turbulent interface or situations where there is significant amplitude of surface fluctuation [as for the capillary-wave case in Saylor and Handler (1997)]. The use of the wave slope may not apply to cases where the interface is relatively quiescent, which is typical for turbulence generated from beneath the interface [for example, the grid stirred tank of George et al. (1994), or the submerged jet-induced experiments of Khoo and Sonin (1992)]. There are also issues relating to accuracy of measurements when the wave slope is almost nonexistent. Furthermore, the use of the wave slope for relating the interfacial mass transfer assumes fundamentally that the wave slope is uniquely related/correlated to $\beta$, which has not been proven thus far, whether experimentally or otherwise. In Duke et al. (1995) it was just stated that the normal velocities caused by waves are directly related to wave slopes, and, hence, it is expected that $\beta$ would be strongly affected by the wave slope as well. Such an assumption may be applicable if a linear relationship exists between the wave motion and the velocity field. The relationship is likely to be nonlinear, however, especially for a more vigorous turbulent interface. Regardless, there is no experiment or theory to support the linear relationship between $\beta$ and the wave slope or even the range of conditions where the said relation is applicable. It is our contention that a robust model for the interfacial mass transfer should be based on directly measured $\beta$. A vertical velocity gradient exists beneath all interfaces, regardless of the turbulence generation mechanisms and/or surface-wave condition.

The interest in $\beta$ as the all-important parameter that controls the scalar transport across the turbulent gas–liquid interface provided the motivation for the development of a technique that can simultaneously measure the fluctuating interface and the flow field beneath it. The almost continuous fluctuation of the interface effectively ruled out the use of conventional Eulerian-based instrumentation like hot-wire anemometer and LDV. Cheung and Street (1988) used a wave-following LDV in their experiment measurement, but this technique has limited range and accuracy. Hassan et al. (1996) and Hering et al. (1998) have proposed techniques based on particle image velocimetry (PIV) with the intention of measuring the interface fluctuations as well as the velocity just beneath it. In the works just mentioned, however, there is only very limited quantification of the velocity fields with respect to the fluctuating interface. Their primary shortcoming lies in the inaccuracy in visualizing and tracking the interface's movement. Using a similar PIV-based technique, Law et al. (1999) achieved greatly improved accuracy in tracking the interface fluctuation and, for the first time, successfully quantified the vertical velocity with respect to the fluctuating interface. A deeply submerged jet was employed to generate the turbulence near the shear-free air–water interface. Therefore, the same methodology can be employed to measure $\beta$ and other surface-influenced parameters at the interface for correlation to the associated scalar transport rate under various flow conditions.

It is the intention of this work to continue on where Law et al. (1999) left off: to measure $\beta$ for two distinct means of turbulence generation close to the gas–liquid interface. One is on turbulence induced directly in the liquid from beneath the interface and the other is associated with turbulence generated from above in the gaseous medium via wind shear. In the midst of such measurements, the mass-transfer experiment is carried out with the aim of providing a common relationship between the rate of scalar transport across the gas–liquid interface, and $\beta$ as the primary hydrodynamic parameter. The selection of these two diametrically different means of turbulence generation in this work belies the hope that the correlation relationship obtained may be applicable to flow pertaining to other means of turbulence generation. (The latter can be broadly construed as a different degree of combination of the two said extreme means of turbulence generation.)

## Experimental Setups

### *Confined jet tank setup and mass-transfer experiment*

For the confined jet tank setup, turbulence is induced/generated in the water and in the region next to the air–water interface from below. The cylindrical test section consists of a vertical plexiglass tank of diameter ($D_t$ of 0.142 m), partially

filled with water up to a level $Z_s$ (see Figure 1; here $Z$ is measured from the nozzle in the vertical direction, and $Z_s$ is the height of the water surface above the nozzle). In this work, experiments were carried out with $Z_s/D_t$ at 3.50, 3.67, and 4.00.

Turbulence is generated in the tank by means of a submerged water jet, placed concentrically with the tank. The jet is directed upward through a nozzle (diameter $d$ of 0.0059 m, thereby giving $D_t/d$ of $\approx 24$) at a volumetric flow rate, $Q$. Water is circulated in a closed loop using a centrifugal pump and the water temperature is kept constant by the heat exchanger. Both the inlet and outlet for the water are located at the bottom of the tank. It has been found previously in Khoo et al. (1992) and Brown et al. (1990) that for such an arrangement, at a distance greater than 3 $D_t$ from the nozzle, the turbulence generated is fairly isotropic on a horizontal plane, with its intensity decreasing with further elevation. The turbulence intensity in the system can be easily varied by varying the momentum flux across the nozzle jet. The system Reynolds number used to characterize the flow condition is defined as

$$Re_s \equiv Q/d\nu \tag{5}$$

where $\nu$ is the kinemetic viscosity. It can also be noted that in previous works with a similar setup (Sonin et al., 1986; Brown et al., 1990; Law et al., 1999), $Re_s$ was established as one of the two important dimensionless parameters characterizing the state of turbulence in the test section and near to the interface. The other parameter is the water level above the nozzle expressed as $Z_s/D_t$. For the present work, the bulk measurements and the near surface characterization are first presented in terms of these two apparatus-related dimensionless parameters for possible comparison. (This is subsequently followed by the selection/use of dimensionless parameter(s) that are *not* expressed directly in terms of apparatus dimension or flow condition based on direct apparatus dimension, with the intention that the same parameters can be used for other means of turbulence generation, as in a wind-induced flow.)

For the mass transfer experiment, a lid closes the cylindrical tank top with inlet and outlet openings for circulation of the gaseous specimen (carbon dioxide in this study). $CO_2$ was introduced at just above the interface and expelled at a higher elevation. The aim is to prevent buildup of any noncondensable gases, notably air, residing close to the interface. Any air in the system, being lighter than $CO_2$, would naturally be

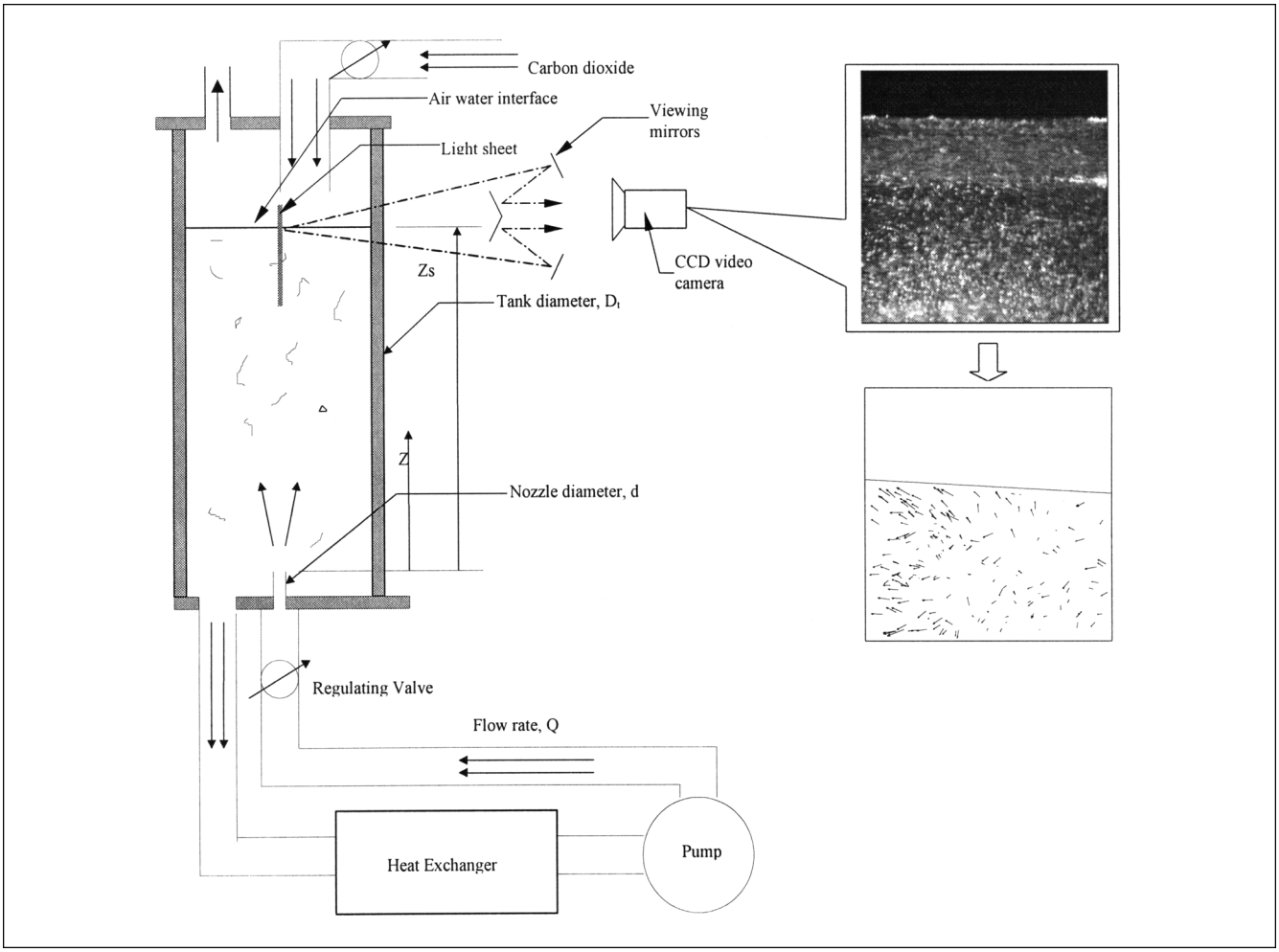


**Figure 1. Confined jet tank setup (not to scale) and optical setup for interface visualization.**

expelled. All the other precautions taken, such as heating the $CO_2$ to make it the same temperature as the bulk water in the test section, running the experiment with $CO_2$ for an initial period of 20–30 min to ensure uniform steady-state initial conditions, and others are fully described in Khoo and Sonin (1992), and so is not repeated here.

### *Circular wind–wave tunnel and mass-transfer experiment*

In the circular wind–wave tunnel, turbulence in the water is generated via wind shear from above. This setup is similar to the "small" circular wind–wave facility used by Jahne et al. (1979, 1987). It consists of an annular water channel with 10-cm depth, 10-cm width with 40-cm ID and enclosed in a 75-cm diameter external cylindrical tank. Each of the sections is made of transparent plexiglass material for access by the laser light source. Wind is produced by means of a rotor with four plexiglass paddles (of 20-cm width) arranged at right angles. In the experiment, water was filled to a depth ($H$) of 7.5 cm in the channel, and the paddles were located 7.5 cm above the water surface. The setup is shown in Figure 2.

For the purpose of reference, the nominal wind speed in the air is assumed to be the same as the paddle speed, taken directly above the center of the 10-cm-wide water channel [just as in Jahne et al. (1979)]. However, it is important to note that in Jahne et al. (1979), the paddles (blades) were different and the clearance between the paddles and the water surface was not mentioned, and, hence, any comparison made can only be qualitatively and in terms of trends. Wind velocity is not measured specifically in this work, and the paddle speed is taken as the wind speed. The use of paddle speed as the parametric indicator of the turbulence generation intensity in the wind–wave tunnel is not dissimilar to the use of the system Reynolds number ($Re_s$) to describe the equivalence for the confined jet experiment. In fact, for characterization of interfacial mass transfer for a low-solubility gaslike $CO_2$, resistance to the gas absorption resides primarily in the liquid side turbulence characteristic near the interface (Jahne and Hau$\beta$ecker, 1998). Accurate measurement of the wind velocity profile is, therefore, deemed not critical, and will not aid in the quantification of the critical parameter (expressed in terms of $\beta$, as shown in the next section) influencing interfacial mass transfer.

For the mass-transfer experiment, the circular wind–wave tunnel can be sealed by a gas-tight lid and flushed with a pure gas specimen ($CO_2$) through the openings at the side. Similar to the confined jet tank experiment, air was expelled through the opening in the lid at the top while $CO_2$ was being introduced. It may be mentioned that the present setup is suitable for the study of interfacial mass transfer, as it is very compact and tends to produce a fairly uniform homogeneous surface condition that is not fetch-dependent like the linear wind–wave facilities.

## Technique for Near-Surface Turbulence Measurement

The technique used for near surface turbulence measurement has being described by Law et al (1999). The technique been validated as being able to accurately measure the interface fluctuation simultaneously with the flow field beneath it. Following is a brief description of the salient feature of the experiment, and interested readers can refer to Law et al. (1999) for details.

This PIV-based technique basically clearly visualizes both the interface and the particle-seeded flow field beneath the interface on a single image. The particle seeding is in the form of 30-$\mu$m polycrystalline particles, while the interface is visualized by introducing fluorescent dye into the liquid. The purpose of the dye is that when a laser light sheet is used to illuminate the visualization plane, the liquid side produces a strong luminance that contrasts very sharply with the air side. The edge of this contrast is the location of the interface. The advantage of visualizing the interface using luminance contrast is that the interface will always show up as a distinctive continuous edge, regardless of surface motion. It should be noted that the dye also produces a luminance intensity that is different from the particle seeding used for PIV. Therefore, when the flow is seeded with both particles and dye, the interface can be located by determining the edge of the luminance contrast between air and water, while the movement beneath the interface can be studied by analyzing the motion of the particles.

For an unobstructed view of the interface and the flow field beneath it, two distinct views need to be captured on a single image. The first view looks up slightly below the surface for complete visualization of the flow field beneath the interface. The other view looks down from a slight angle above the surface for an unobstructed view of the interface. Figure 1 shows the arrangement of viewing mirrors to produce these two distinct views in a single image. An interface edge detection tracking technique is then applied to the image to determine the profile as well as the fluctuation of the interface. The movement of the interface is deduced by tracking the change of interface location between images taken at a known time interval.

The velocity field beneath the interface is measured by the well-established PIV method. The tracking algorithm used in this experiment first employs the digital particle image velocimetry (DPIV) technique of cross-correlation between interrogation cells to obtain an approximate velocity vector. Using the result obtained as a guide, one then tracks the displacement of an individual particle found within the interrogation cell [similar to the particle tracking technique (PTV) used in Khoo et al. (1992), but with an extended dynamic range via the use of a mechanical shutter to control the time interval between images]. In this way, the velocity vectors obtained have better accuracy as well as spatial resolution than if based on the traditional DPIV or PTV only. Figure 1 shows a typical captured image and the processing to obtain the distinct continuous interface and the velocity vectors in the liquid.

## Mass-Transfer Rate Measurement

Mass-transfer rate ($K_L$) measurement, using $CO_2$ as the specimen, is carried out in both setups. The equation governing the transfer of $CO_2$ into the liquid volume in the test systems is

$$V\frac{dC}{dt} = K_L A(C_s - C) \tag{6}$$

**Table 1. Variation of Sc Number and Other Properties with Glycerol in the Mixture**

| Glycerol % by Vol. at 27°C | 0 | 13 | 22 |
|---|---|---|---|
| $\nu \times 10^6$ ($m^2/s$) | 0.8588 | 1.101 | 1.758 |
| $D \times 10^9$ ($m^2/s$) | 2.047 | 1.374 | 1.095 |
| Sc | 418 | 801 | 1605 |
| $C_s \times 10^2$ (mol/L) | 3.304 | 2.855 | 2.593 |

where $V$ is the volume of water in the test system, $A$ is the area of the interface, $C$ is the bulk concentration of $CO_2$ in water, and $C_s$ is the saturation concentration of $CO_2$ at the interface. In this work, the volume of liquid in the confined jet tank varies accordingly to the water level set at $Z_s/D_t =$ 3.5, 3.67, and 4.0. On the other hand, the volume of water in the circular wind–wave tunnel is the same for a given water depth of 7.5 cm. Under steady-state conditions, Eq. 6 becomes

$$K_L = V/At_f \ln\left[(C_s - C_i)/(C_s - C_f)\right] \tag{7}$$

where $C_i$ is the initial concentration of $CO_2$ in the water, and $C_f$ is the final concentration after time $t_f$. By measuring $C_i$ and $C_f$, the liquid-side mass-transfer velocity ($K_L$) can be determined. In this work, the $CO_2$ concentration in the liquid is measured using gas chromatography (estimated accuracy $\pm 1\%$), with samples taken from the system at the beginning and at the end of each run, each of which lasts between 1 and 5 h, depending on the turbulence conditions imposed. Concentrations $C_i$ and $C_f$ were obtained as the average values of 10 samples, with a variation found to be well below 5%.

In the confined jet tank experiment, $K_L$ is also measured for different water–glycerol mixtures (0%, 13%, and 22% by volume). The reason for using a water–glycerol mixture is to produce different Schmidt-number (Sc$\equiv \nu$/D) conditions for correlation to $K_L$. With pure water at 27°C, the Sc number for $CO_2$ is $\approx 420$. At 13% and 22% volume of glycerol, the Sc number is $\approx 800$ and $\approx 1600$, respectively (see Table 1). The viscosity was determined using a HAAKE Rheometer

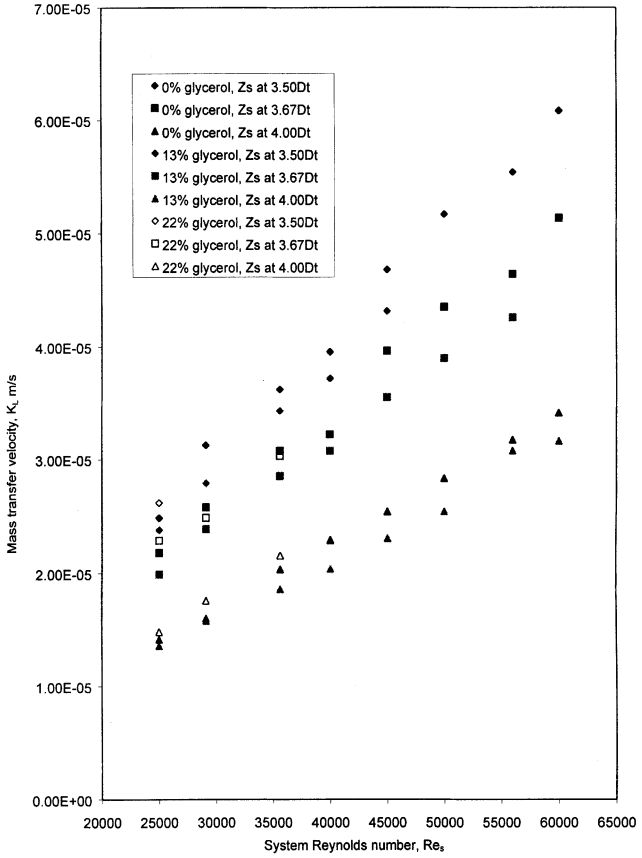


**Figure 3. Mass-transfer velocity for $CO_2$ gases, measured in the confined jet tank with different percentage of glycerol, $Z_s/D_t$ and $Re_s$.**

within an accuracy of $\pm 2\%$. The diffusion coefficient and saturation concentration of $CO_2$ in the liquid were obtained from Davidson and Cullen (1957), Cox and Head (1962), and Brignole and Echarte (1981). Khoo et al. (1992) employed a similar scheme of achieving a different Sc condition without using a different gas specimen in a similar study of air–water

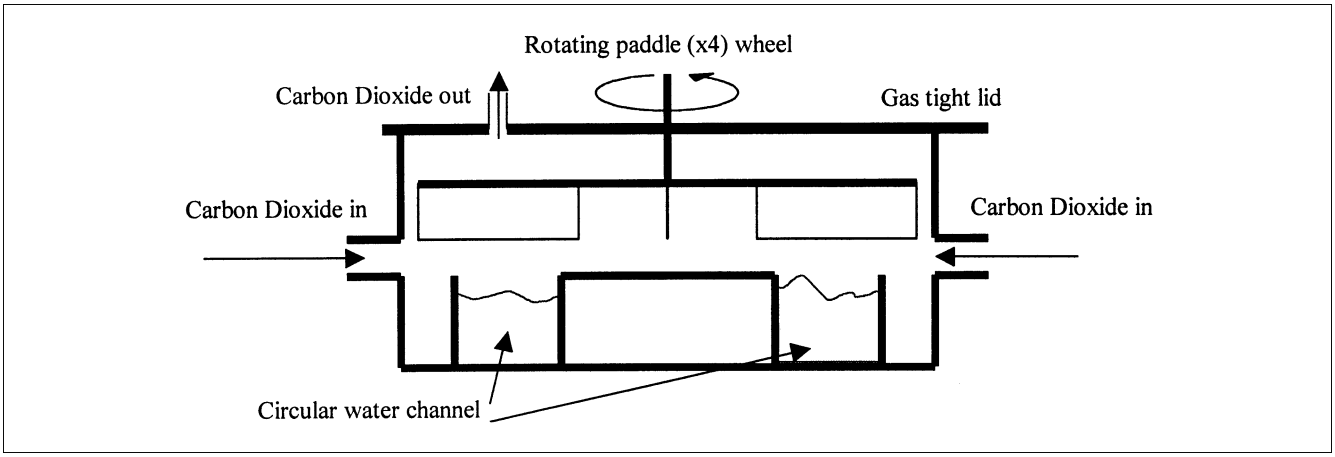


**Figure 2. Circular wind–wave tunnel (not to scale).**

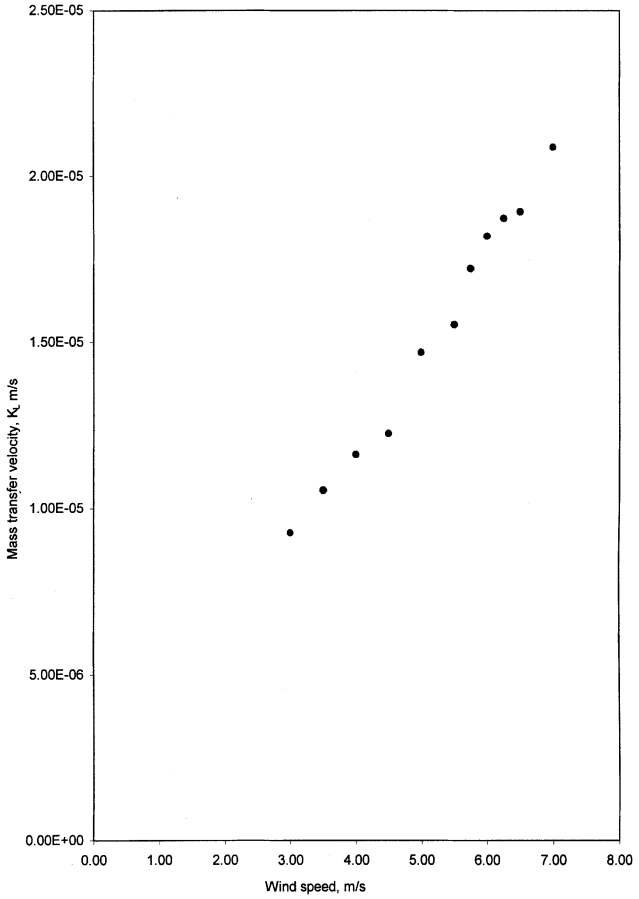


**Figure 4. Mass-transfer velocity for $CO_2$, measured in the circular wind–wave channel.**

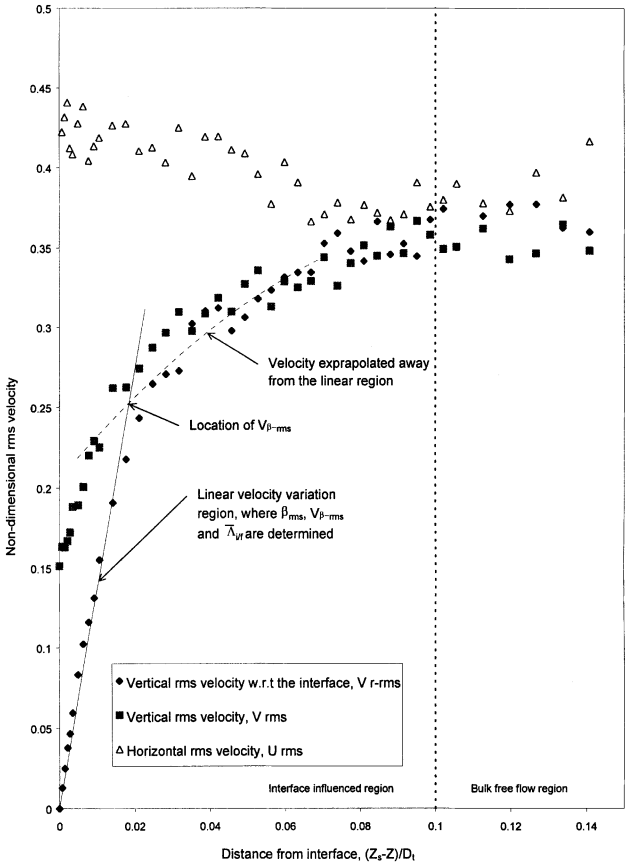


**Figure 5. Typical velocity profiles near the interface in the confined jet tank.**

Velocity is made nondimensional using $Q/Dd$.

mass transfer. The mass-transfer rate measurements were usually carried out separately from flow measurements, and it is absolutely essential and critical to keep the interface clean. In fact, precautions were taken to clean the interface using suction as well as lens paper to skim off any possible trace of surfactants at the beginning of each experiment. For the experiment on turbulence measurement, one still has to ensure that the fluorescent dye and particles were well mixed homogeneously in the flow field, and that no visible trace of the particles appear "floating" on the liquid surface. (Strictly, the extremely diluted content of the particle seeding and fluorescent dye theoretically should not have any effect on the mass-transfer experiment, but such a simultaneous experiment was not attempted.)

Figure 3 shows the variation of $K_L$ with system Reynolds number $Re_s$ in the confined jet tank. It is observed that for a fixed $Z_s/D_t$, the mass-transfer velocity for a given glycerol–water mixture increases rather linearly with the system Reynolds number, $Re_s$ (which is a measure of the turbulence intensity). In particular, the behavior of the linear plot(s), which passes through the origin in the pure-water case (not specifically depicted in the figure), is consistent with the work of Khoo and Sonin (1992).

The mass-transfer velocity for the wind-induced turbulence in the circular wind–wave tunnel is shown in Figure 4. Here $K_L$ is found to increase with the wind speed in a fairly linear manner. This concurs with the results obtained in a linear wind–wave tunnel by Broecker and Siems (1984), who performed the investigation for $O_2$ and $CO_2$ species. Although the result in Figure 4 shows linear behavior, which if extrapolated, passes close to the origin, the data of Broecker and Siems (1984) indicate a linear intercept very distinct from the origin. This can be attributed to the presence of fetch in a linear wind–wave tunnel. The mass-transfer data measured by Jahne et al. (1979, 1987) in a similar type of circular wind–wave setup also shows linear behavior with an intercept through the origin, although a quantitative comparison may not be so meaningful. It can be noted, however, that when the same data for $K_L$ are plotted against interfacial shear velocity based on liquid density ($u^*$), they exhibit a linear trend and concur reasonably well quantitatively with Jahne et al. (1979, 1987) for the lower range of $u^*$ before the "break." The figure is not provided here, but is given in Law (2002) for reference by interested readers. [Anyway, the intent of this section is only to show broad concurrence of the mass-transfer results when plotted against commonly used bulk parameters employed to characterize the state of turbulence near the interface on the liquid side. Direct measurements of the important turbulence structure next to the liquid interface for correlation are described in the following section.] Quite interestingly, both Broecker and Siems, and

Jahne et al. found that there are two linear regimes for the $O_2$ and $CO_2$ gases tested, even as $K_L$ increases with the wind speed. It was suggested that the presence of the second linear region at the higher wind speed is due to the presence of wave breaking (and the possible consequent presence of bubbles generated in the flow). In this work, measurements are deliberately taken for the range before the occurrence of wave breaking, and, hence, it is not surprising there is no observation of different regimes. (The onset of wave breaking at a much higher wind speed and associated mean flow in the water below is currently beyond the dynamic range of the present PIV configuration for the measurement of $\beta$.)

## Interface Turbulence Structure

### *Confined jet tank*

Velocity measurements of the flow field very close to the interface for the turbulence induced by the confined jet were carried out. Figure 5 shows a typical velocity profile for the case of pure water (0% glycerol) with $Z_s/D_t = 3.50$, and $Re_s = 56{,}000$. (Here the velocity is made dimensionless using $Q/D_t d$.) Around 0.1 $D_t$ from the interface, the horizontal ($u$) and vertical ($v$) rms velocities are equal to each other to within $\pm 10\%$; both $u_{rms}$ and $v_{rms}$ are found to decrease together and uniformly with $Z$ in the bulk-free region. This shows that the flow is practically isotropic on the horizontal plane, which agrees with previous investigations using a similar setup (Brown et al., 1990). Toward the surface-influenced interface region ( $< 0.1$ $D_t$ from the interface and termed the interfacial or surface-influenced layer), the trend of the vertical rms velocity diverges from the horizontal rms velocity. The former is increasingly damped, and its kinetic energy is imparted to the velocity component parallel to the interface. This is shown by the increase in horizontal rms velocity toward the interface, while the vertical rms velocity decreases. At the interface, the vertical velocity component assumes the velocity of the fluctuating interface ($v_{i\text{-}rms}$). This velocity variation is fairly typical for turbulence generated from beneath the interface. In an earlier study, Law et al. (1999) described the velocity variation in great detail with extensive comparisons made to other works in the literature and is not repeated here.

Also shown in Figure 5 is the profile of the vertical velocity variation taken with respect to the fluctuating interface. This is possible because of the simultaneous measurement of the interface movement and the flow field beneath it. The velocity with respect to the interface, $v_r$, is determined by subtracting the interface movement from the velocity $v$ measured, that is

$$v_r = v - v_i \tag{8}$$

where $v$ is the measured flow velocity and $v_i$ is the velocity of the interface *directly above* the velocity vector in consideration. It is observed that near the interface, the profile of $v_{r\text{-}rms}$ departs increasingly from $v_{rms}$ and assumes the null value at $Z_s$. Further away from the interface, the difference between $v_{r\text{-}rms}$ and $v_{rms}$ becomes smaller. It is most interesting and very important to note that in the immediate vicinity of the interface region, the variation of $v_{r\text{-}rms}$ is fairly linear. This is in agreement with McCready et al.'s (1986) analysis indicating that close to a mobile interface, the variation of vertical velocity with depth is approximately linear, $v_r = \beta Z$. From the profile of $v_{r\text{-}rms}$ (Figure 5), several new parameters important to mass-transfer modeling are proposed below.

We define $\beta_{rms}$ as the slope of the vertical rms velocity fluctuation with respect to the interface ($v_{r\text{-}rms}$). A possible velocity and length scale in the immediate vicinity of the interface are $v_{\beta\text{-}rms}$ and $\overline{\Lambda}_{i/f}$, respectively; $v_{\beta\text{-}rms}$ and $\overline{\Lambda}_{i/f}$ quantified the extent of the linear variation of $v_{r\text{-}rms}$ such that

$$\beta_{rms} = v_{\beta\text{-}rms}/\overline{\Lambda}_{i/f} \tag{9}$$

Here $\overline{\Lambda}_{i/f}$ is the distance from the interface where the linearity of $v_{r\text{-}rms}$ still holds. The terms $v_{\beta\text{-}rms}$ and $\overline{\Lambda}_{i/f}$ represent the velocity and length scales, respectively, at which $v_{r\text{-}rms}$ departs from the linear behavior and are constant for a given experiment. [In the determination of $\overline{\Lambda}_{i/f}$, it is taken to be the intersection of the linear extent with the extrapolated behavior of $v_{r\text{-}rms}$ within the surface-influenced region (see Figure 5). The linear extent through the origin is obtained with data points that give an $R^2$ (coefficient of determination for linear regression) greater than 0.95.] It is important to mention that the (dimensional) parameters defined above are measured and are not assumed direct apparatus dimension dependent or flow condition dependent directly on apparatus dimension and setup. As such, they are essential to the possible development of universal dimensionless grouping(s) controlling the transport rate across the turbulent gas–liquid interface, which is also independent of the turbulence generation process whether be it induced from below or from above the surface. $\beta_{rms}$ has the unit L/time and can be expressed in the following nondimensional form

$$\beta^+_{rms} \equiv \frac{\beta_{rms}\nu}{v^2_{\beta\text{-}rms}} \tag{10}$$

where $\nu$ is the kinemetic viscosity. This nondimensional $\beta_{rms}$ encompasses all three parameters ( $\beta_{rms}$, $v_{\beta\text{-}rms}$, and $\overline{\Lambda}_{i/f}$) that define the hydrodynamic characteristics in the small linear region at the interface. Even though $\overline{\Lambda}_{i/f}$ does not appear explicitly in the nondimensionalisation, its influence is implicit via $\beta_{rms}$, as in Eq. 9. As may be reiterated, the concentration boundary layer next to the interface for a less soluble gas like $CO_2$ is very thin, and, hence, the hydrodynamic features residing in this region are deemed essential determinants controlling the transport rate. Alternatively, one can rearrange and define $\beta^+_{rms}$ as

$$\beta^+_{rms} \equiv \frac{\nu}{v_{\beta\text{-}rms}\overline{\Lambda}_{i/f}} \tag{11}$$

which can be constructed as the inverse of the familiar Reynolds number. Figures 6 and 7 show the variation of $\beta^+_{rms}$ and $\overline{\Lambda}_{i/f}/D_t$ with the system Reynolds number $Re_s$ for the confined jet tank. It is clear that for a given water–glycerol mixture and same $Z_s/D_t$, $\beta^+_{rms}$ decreases with $Re_s$. Viewed from Eq. 11, it is interesting to note that an increase in the system Reynolds number (a measure of the macro/large-scale

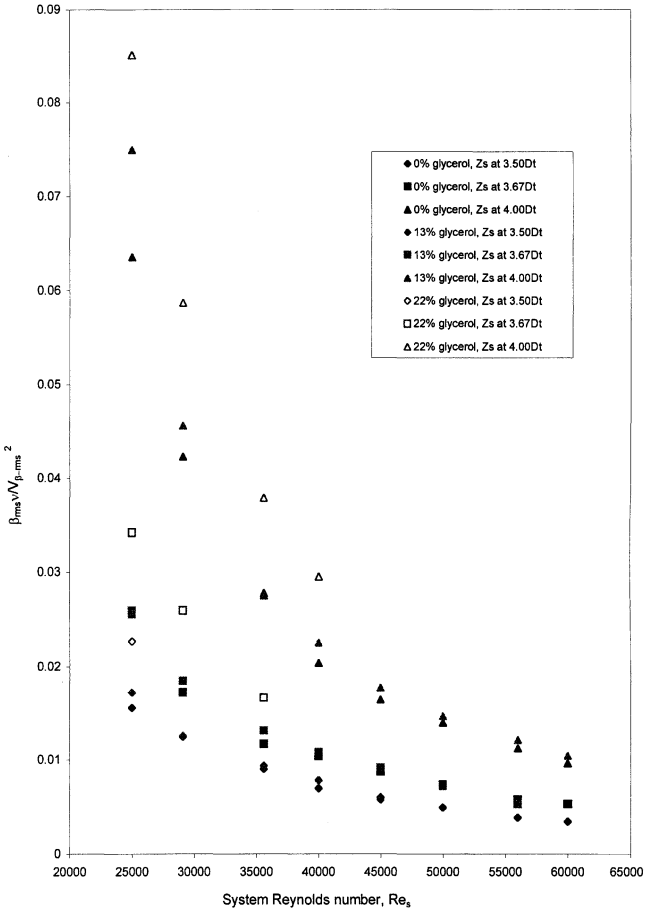


**Figure 6. Variation of nondimensional $\beta_{rms}$ ($\beta^{+}_{rms}$) in the confined jet tank.**

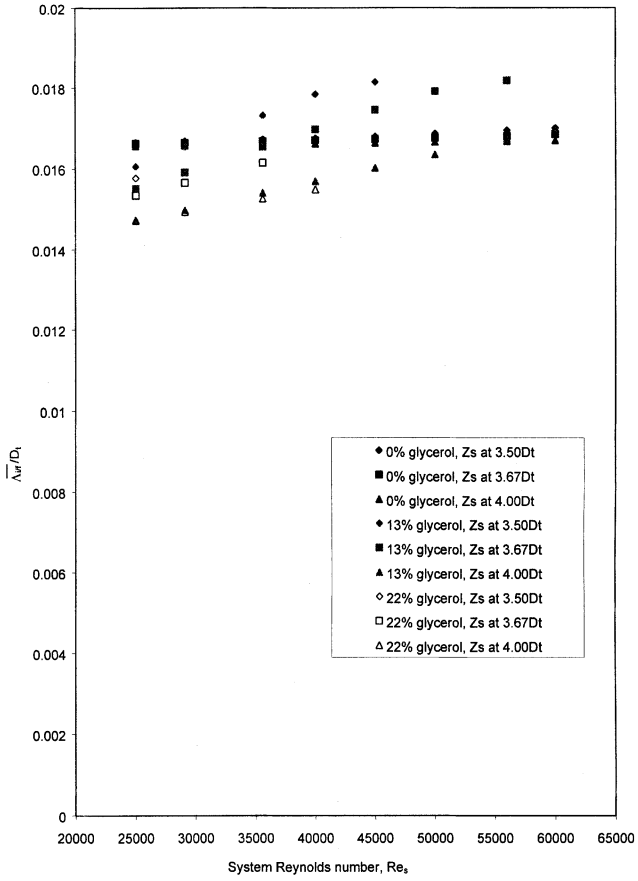


**Figure 7. Variation of $\overline{\Lambda}_{i/f}/D$ with $Re_s$ in the confined jet tank.**

parameters) has given rise to a corresponding increase on $1/\beta^{+}_{rms}$, which is a measure of the micro/small-scale Reynolds number. One can also observe that the general effect of increasing glycerol concentration has led to an increase in $\beta^{+}_{rms}$ while keeping $Re_s$ and $Z_s/D_t$ fixed.

The behavior of $\overline{\Lambda}_{i/f}/D_t$ with $Re_s$ as shown in Figure 7 indicates a rather weak dependence. Such observation is perhaps not surprising, as one can expect $\overline{\Lambda}_{i/f}$ to be influenced somewhat by the macroscale in the system. Earlier works (Khoo et al., 1992; Law et al., 1999) have shown that a constant integral length scale, proportional to the tank diameter, exists in the bulk region of the confined jet tank. One would therefore expect the length scales to be influenced by the tank dimension, rather than $Re_s$. It should be mentioned that $\overline{\Lambda}_{i/f}$ is much smaller than the turbulent macroscale of the bulk region $\Lambda_g$, where

$$\overline{\Lambda}_{i/f} \approx 0.275\Lambda_g \tag{12}$$

Here $\Lambda_g$ is the transverse integral length scale of $0.062D_t$, as found in Law et al. (1999).

### *Circular wind–wave channel*

Figure 8 shows the typical near-surface velocity variation in the circular wind–wave channel with a nominal wind speed of 5 m/s. It can be seen that the velocity profile under the wind–wave generation mechanism differs significantly from the confined jet tank case where turbulence is generated from beneath the interface. The wind shearing across the interface produces a strong mean flow ($U_{\text{mean}}$) in the direction of the wind, which decreases in magnitude with the depth beneath the interface (not shown). The rms velocities in Figure 8 are made dimensionless with respect to the streamwise mean interfacial shear velocity ($u^*$). Here $u^*$ is obtained from the gradient of the mean streamwise velocity profile in the liquid measured at close distribution at the interface (see also Rashidi and Banerjee, 1988).

Both the horizontal rms velocity fluctuation and the vertical rms velocity fluctuation have large intensities near the interface and decay rather rapidly with depth. Such behavior is very typical for a wind-generated turbulence interface, where the surface wave constitutes a high velocity fluctuation near the surface. It is noted further that both the horizontal and vertical rms velocities share a fairly similar magnitude for the whole spatial distribution. This is quite unlike the case of turbulence generated from beneath the interface, where the interface "damps" the vertical velocity fluctuation and results

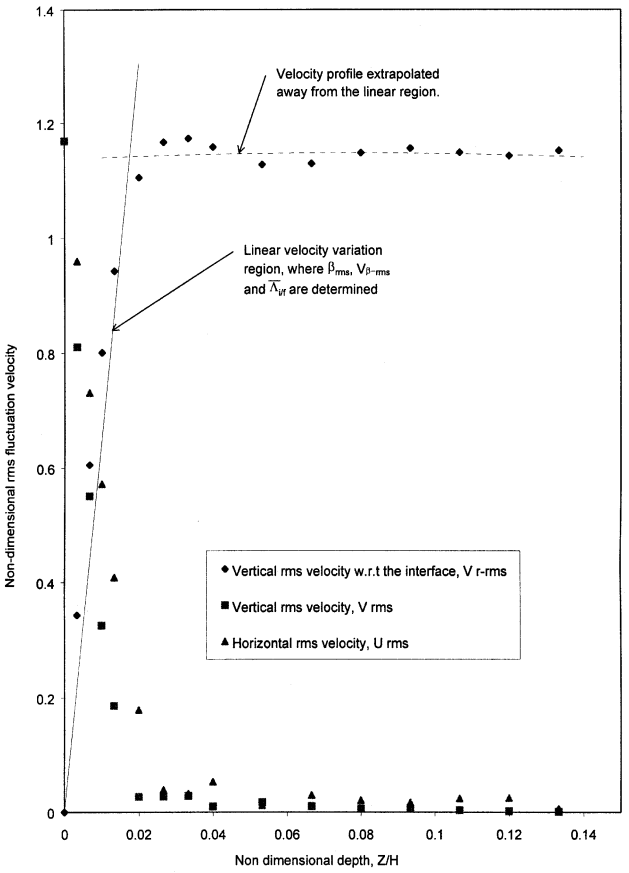


**Figure 8. Typical velocity fluctuation for the region very near the interface of the wind–wave channel.**

Velocity is made nondimensional using the mean interfacial shear velocity, $u^*$.

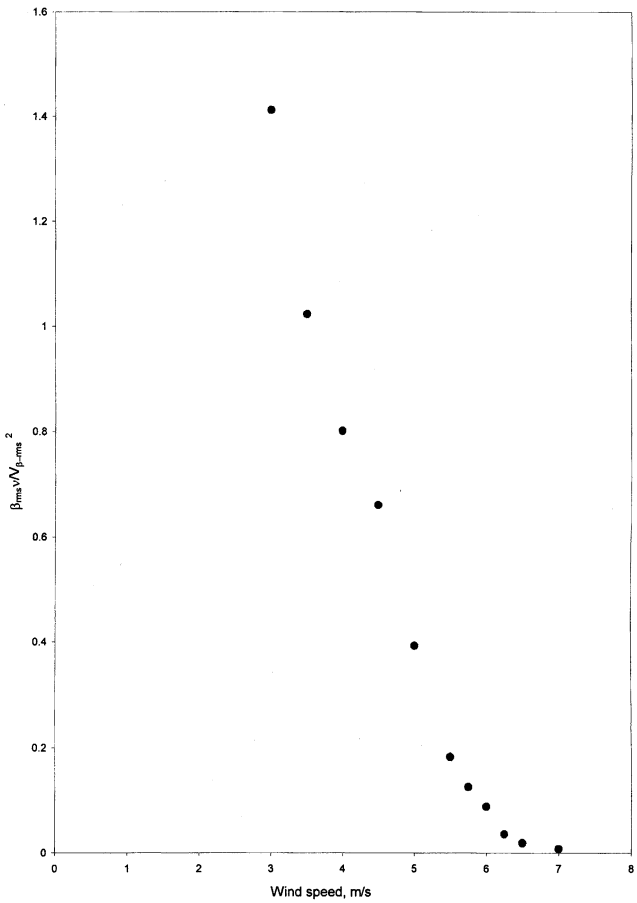


**Figure 9. Variation $\beta^+_{rms}$ in the circular wind–wave tunnel.**

in a transfer of kinetic energy to the transverse component, causing the latter to increase toward the surface.

As in the confined jet experiment, the vertical velocity fluctuation is determined ($v_{r\text{-}rms}$) with respect to the interface. As shown in Figure 8, $v_{r\text{-}rms}$ is equal to zero at the interface and increases with depth to a quantity close to the value of the interface vertical velocity fluctuation, $v_{i\text{-}rms}$. It can also be observed that this profile takes on fairly linear behavior right next to the interface. Using the same approach as for the confined jet experiments, $\beta_{rms}$, $v_{\beta\text{-}rms}$ and $\overline{\Lambda}_{i/f}$ for the wind–wave channel are determined from the $v_{r\text{-}rms}$ profile.

Figures 9 and 10 show the variation of $\beta^+_{rms}$ and $\overline{\Lambda}_{i/f}/H$ with wind speed. It is observed that $\beta^+_{rms}$ decreases fairly rapidly with increases in wind speed. If one holds the view that an increase in wind speed is equivalent to an increase in the imposed flow Reynolds number, then this feature is similar to that found for the confined jet experiment as depicted in Figure 6. The variation of $\overline{\Lambda}_{i/f}$/H, as shown in Figure 10, however, shows a distinct difference from the confined jet experiments. Here, $\overline{\Lambda}_{i/f}/H$ shows a significant increase with wind speed. This can be attributed to the fact that, while there is a fixed macroscale associated with the apparatus for the confined jet experiment and may have influenced $\overline{\Lambda}_{i/f}/D_t$ to behave almost like an invariance, there is none for the circular wind–wave channel. $\overline{\Lambda}_{i/f}/H$ depends very much on the surface-wave condition. The increase of $\overline{\Lambda}_{i/f}/H$ as shown in Figure 10 is in line with the observation that the surface wave became "rough" at a higher wind speed (Jahne et al., 1979, 1987).

## Mass-Transfer and Near-Surface Turbulence Parameter

In the scalar transport of a low solubility gas across the turbulent gas–liquid interface, the resistance lies mainly in the liquid phase, and the typical concentration boundary-layer thickness is usually very thin (much thinner than the associated momentum boundary-layer thickness) next to the interface. As such, it is not unreasonable to suggest that the rate of transport can be expressed as depending directly on hydrodynamic parameters defined for the interfacial region, like $\beta_{rms}$ and $v_{\beta\text{-}rms}$ (with $\beta_{rms}$ and $v_{\beta\text{-}rms}$, $\overline{\Lambda}_{i/f}$ is automatically defined and is no longer an independent variable), and the fluid properties of $\nu$, $D_t$, and $\rho$. By the scaling argument carried out previously in Sonin et al. (1986) and Khoo and Sonin (1992), we can establish that

$$\frac{K_L}{v_{\beta\text{-}rms}} = f\left(\frac{\beta_{rms}\nu}{v_{\beta\text{-}rms}{}^2}, Sc\right) \tag{13}$$

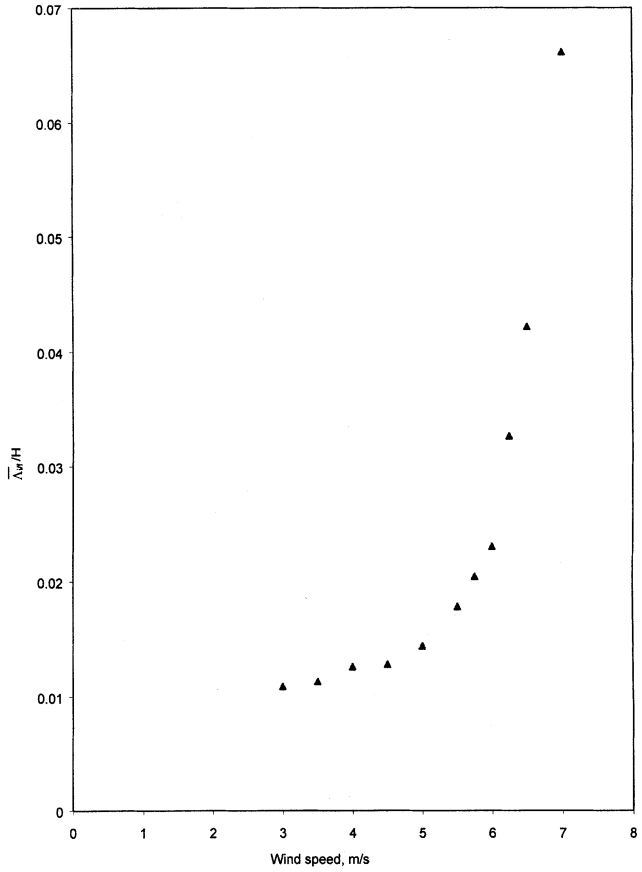


**Figure 10. Variation of $\overline{\Lambda}_{ift}/H$ with wind speed in the wind–wave channel.**

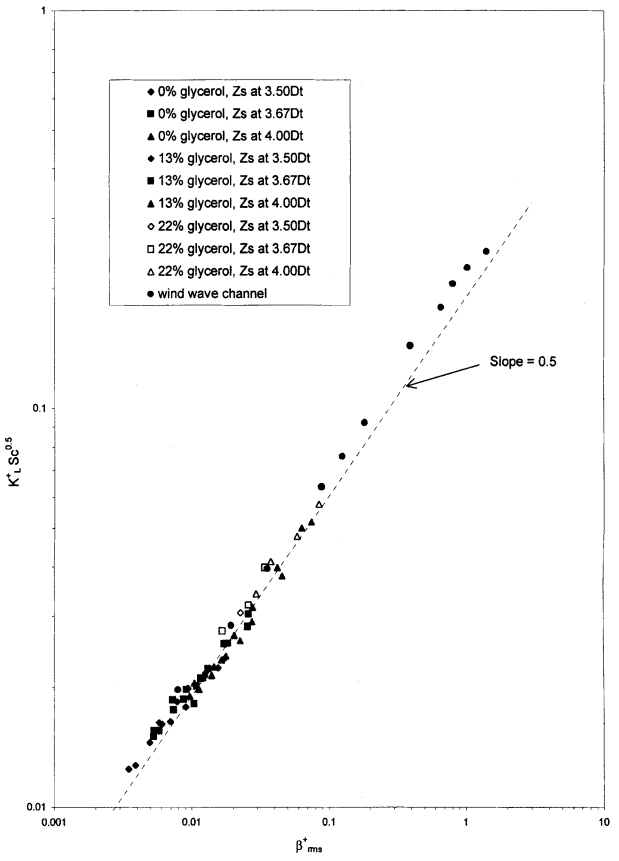


**Figure 11. Relationship between mass transfer and near-surface turbulence parameter.**

where $Sc = \nu/D$ is the Schmidt number. Following the work of Khoo and Sonin (1992), where it was reviewed and discussed that most models developed for interfacial transport [including the prominent large-eddy model of Fortescue and Pearson (1967), and the small-eddy model of Lamont and Scott (1970)] suggest an explicit dependence on $Sc^{-0.5}$, we therefore have

$$\frac{K_L}{\upsilon_{\beta\text{-}rms}} = f\left(\frac{\beta_{rms}\nu}{\upsilon_{\beta\text{-}rms}^2}\right) Sc^{-0.5} \tag{14}$$

Defining $K_L^+$ as the nondimensional mass transfer rate, $K_L/\upsilon_{\beta\text{-}rms}$, Eq. 14 can be expressed in terms of nondimensional parameters

$$K_L^+ Sc^{0.5} = f(\beta_{rms}^+) \tag{15}$$

where $\beta_{rms}^+$ is the nondimensional $\beta_{rms}$ as defined in Eq. 10. Figure 11 shows the plot of $K_L^+ Sc^{0.5}$ against $\beta_{rms}^+$ on a log-log scale for all the data collected for *both* the confined jet tank and the circular wind–wave tunnel. The best-fit line for the data shows a linear slope of gradient with a magnitude close to 0.5 (with an $R^2$ coefficient of 0.98); this indicates a dependence on $(\beta_{rms}^+)^{0.5}$ for the mass-transfer rate. Hence, the mass-transfer model using interfacial turbulent parameters takes the functional form

$$K_L^+ = f\left((\beta_{rms}^+)^{0.5}\right) Sc^{-0.5} \tag{16}$$

On a linear plot of $K_L^+ Sc^{0.5}$ vs. $(\beta_{rms}^+)^{0.5}$, as depicted on Figure 12, the linear behavior (of slope $\approx 0.22$ with an $R$-square coefficient of 0.98) that passes through the origin can be realized. This gives rise to the proposed relation

$$K_L^+ Sc^{0.5} = 0.22\,\beta_{rms}^{+\,0.5} \tag{17}$$

This functional relationship between $K_L^+$ and $\beta^{+0.5}$ is very similar to that derived by McCready et al. (1986). McCready et al. carried out a computer simulation for a flat mobile interface by assuming the presence of eddies with a vertical velocity characterized by

$$v \approx y\beta(t)\cos\left(\frac{2\pi Z}{\lambda}\right) \tag{18}$$

where $Z$ is the transverse coordinate and $\lambda$ is the typical eddy size. These authors had to employ a certain random function for $\beta(t)$, since it was not available experimentally or otherwise. Even then, a functional form for the mass-transfer rate almost identical to Eq. 17 is obtained except for the interfacial shear velocity used by McCready et al. for the nondimensionalization of $\beta$ (this is for their comparison to mass-transfer data measured in liquid-film flow). It can be noted, however, that McCready et al. derived a coefficient of 0.71, which is fortuitously the same order of magnitude as in

Eq. 17, considering that there are several assumptions utilized in the derivation. (Closer examination of Eq. 17 and the expression by McCready et al. shows that the velocity-scale term used in the nondimensionalization or description of the near-surface turbulence drops out and does not appear in the final form.) McCready et al. also found that the mass-transfer rate is only very weakly dependent on the scale of turbulence.

The remarkable agreement between data from the confined jet tank and the circular wind–wave tunnel shows the possible existence of a single universal model/correlation for interfacial mass transfer for turbulence conditions generated by vastly different means. The existence of a universal correlation is incumbent on the concurrence of the mass-transfer data from the two extreme spectrums of turbulence generation in the liquid: one from above the interface, and the other from beneath the surface. Other means of turbulence generation can be broadly understood as differing degrees of combination of these two ends of the spectrum. This is a necessary step in obtaining a possible universal correlation, although not sufficient to ensure its existence, and many experiments of different means of turbulence generation are necessary to ascertain its applicability. It should be mentioned that a relationship as proposed in Eq. 17 has an advantage over other models. The existing models normally employed parameters specific to the flow conditions in the bulk region and related to the ways of generating turbulence or geometrical dimensions. Application or the extension of such a model to other flow conditions is not always possible or straightforward.

The establishment of $\beta$ as the important parameter governing the transport rate across the interface, as in Eq. 17, provides support to the idea of a small-eddy model. Measured quantities like $\beta$ and $v_{\beta\text{-}rms}$ are found in a small region limited by $\overline{\Lambda}_{i/f}$, and $\overline{\Lambda}_{i/f}$ is understood to be more closely associated with the small-eddy structure. One should be aware that the small-eddy model first proposed by Lamont and Scott (1970) supposedly has a small length scale, such that

$$l_s \approx \left(\frac{\nu^3}{\epsilon}\right)^{1/4} \tag{19}$$

where $\epsilon$ is the rate of turbulence dissipation. Two difficulties arise immediately. First, the relationship in Eq. 19 is based on the Kolmogorov universal equilibrium theory, and it is assumed that these small-scale motions are statistically independent of the large scale, as in an isotropic turbulent flow (or not so nearly isotropic turbulent flow, but still with local isotropy). Concerns arise if this is equally true in a highly anisotropic turbulent flow next to the interface where there may not even be local isotropy. Second, even if Eq. 19 is valid, there is no means of measuring $\epsilon$ in the anisotropic region next to the interface. [Even for the much simpler configuration of anisotropic turbulence next to a flat solid surface, there is no known measurement technique capable of evaluating $\epsilon$ as discussed in Khoo et al. (2000).] Therefore, it is perhaps not surprising that the "small-eddy" model, as interpreted and applied in the traditional sense, has not been particularly successful in its potential role as a universal model for the turbulence transport across the interface. (One can view the traditional small-eddy model as eddies of the Kolmogorov microscale based on turbulence conditions in the bulk of the liquid where isotropy (or local isotropy) is assumed to be valid. Evaluation does not pertain directly to the turbulence condition in the strong anisotropic region next to the interface.) For the present work, it can be construed that the parameters in Eq. 17 pertain directly to the state of turbulence at the interface and are likely to be associated with the characteristics of the small eddies residing next to the surface.

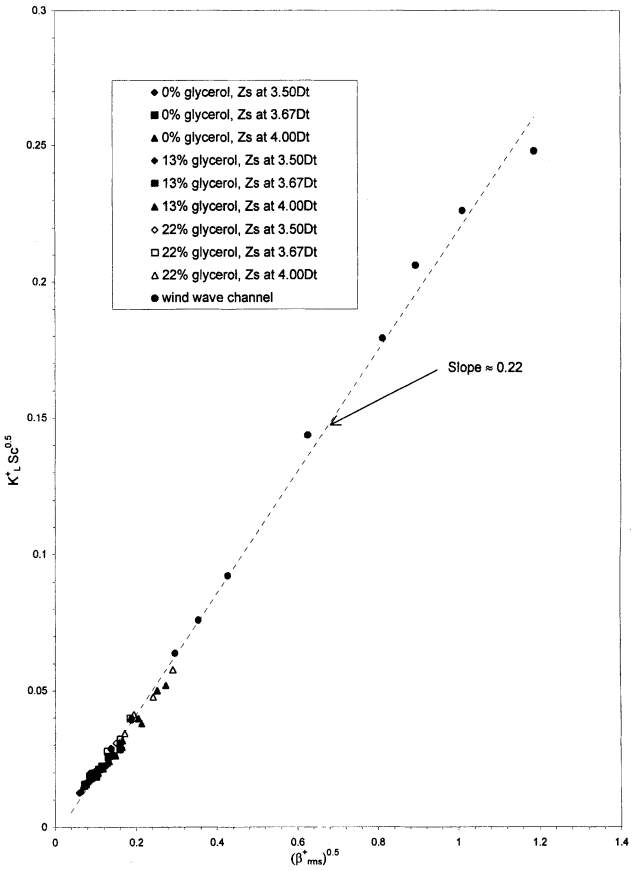


**Figure 12. Linear relationship between mass transfer and near-surface turbulence parameter.**

The association of Eq. 17 with the small-eddy model does not necessarily imply that the large-eddy model is of no consequence. In isotropic turbulence, the usual energy cascading process from the (large) macroscale through the inertial subrange to the (small) Kolmogorov microscale exists. Even in an anisotropic turbulence region, there is presumably some relation between the large- and small-scale eddies. If such a general relationship exists for the near-surface turbulence, one may be able to relate uniquely the respective dimensionless groupings containing hydrodynamic parameters associated with the large-scale and small-scale eddies. A possibility therefore exists that the large-eddy model can be universally applied to explain the rate of turbulent transport across the interface. This leads us to the investigation in the next section.

## Possible Relationship Between $\overline{\beta}^+_{rms}$ and Other Near-Surface Macroscale Turbulence Quantities

Besides attempting to establish a unique relationship, if any, between the small-eddy model expressed in term of $\beta^+_{rms}$

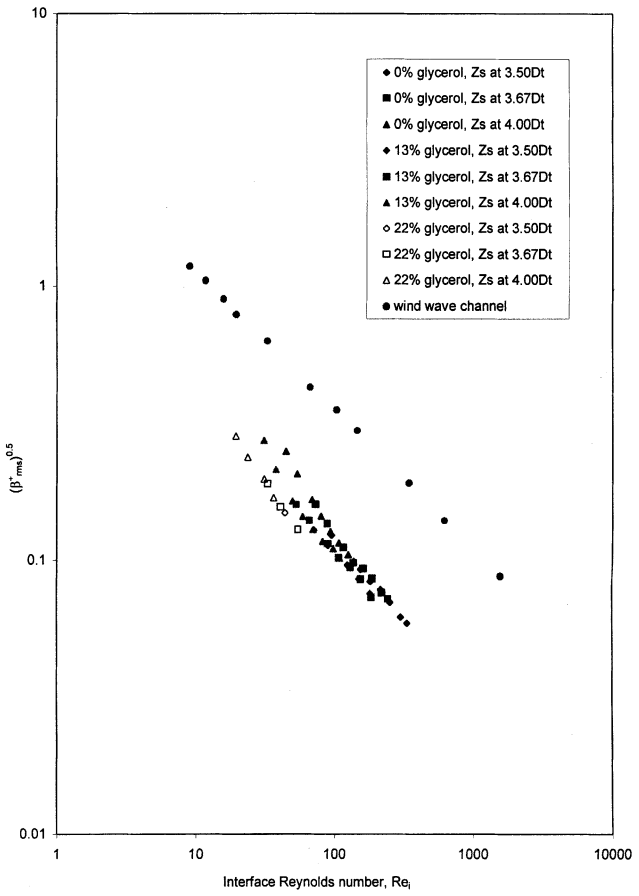


**Figure 13. Correlation between $\beta^+_{rms}$ and interface Reynolds number.**

and the large-eddy model, it is also imperative and practical to relate $\beta^+_{rms}$ to a group of easily measurable bulk hydrodynamic parameters. Even as Eq. 17 has been shown to be generally applicable to the two vastly different means of turbulence generation, turbulence quantities like $\beta^+_{rms}$ are certainly not easily measured. Any relation to more commonly used bulk hydrodynamic parameters (or easily measured using conventional instrumentation) would prove invaluable and also serve as an effective constitutive relation for turbulence modeling and prediction of the passive scalar transport across the interface. In this regard, the near-surface bulk hydrodynamic parameters selected are $\Lambda_i$ (the transverse integral length scale at the interface) and $v_{i\text{-}rms}$ (the interface vertical velocity fluctuation). (A commonly used term like mean shear velocity at the interface as in a wind-driven flow is not adopted in order to accommodate flow conditions where there is no mean shear at the surface.) Here $\Lambda_i$ is defined as

$$\Lambda_i \equiv \int_0^\infty g(x)\, dx \tag{20}$$

where $g(x)$ is the spatial correlation of the vertical velocity vectors with transverse separation distance $(x)$. A possible dimensionless grouping is the interface Reynolds number,

$$Re_i \equiv \frac{\Lambda_i v_{i\text{-}rms}}{\nu} \tag{21}$$

for our correlation to $\beta^+_{rms}$. Figure 13 shows the distribution of $(\beta^+_{rms})^{0.5}$ vs. $Re_i$. (We have deliberately used $(\beta^+_{rms})^{0.5}$ for the ordinate so that direct reference can be made between $K_L^+ Sc^{0.5}$ and $Re_i$ via Figure 12 for interested readers.) It is apparent that Figure 13 indicates two general but separate regimes: one for the turbulence induced by the submerged jet from beneath the liquid, and the other associated with the wind-shear-induced turbulence from above. There is *no* single universal relationship. By associating $Re_i$ with the large-scale eddy model, it is suggested that the small-scale and large-scale eddy models are not uniquely related and the latter are dependent on the turbulence generation mechanism. This is perhaps not surprising, since the means of turbulence generation, be it wind-shear-induced or otherwise, is known to have a direct bearing on the large-scale eddies and the (mean) bulk hydrodynamic parameters. Therefore, it follows that any attempt to relate the rate of scalar transport to the (near-surface) bulk hydrodynamic parameters in a generally consistent manner is not possible.

Finally, it should be noted that one can select a more commonly used and possibly natural velocity parameter in place of the $v_{i\text{-}rms}$ in Eq. 21 for relating to $\beta^+_{rms}$. For example, the interface mean shear velocity for the case of wind-induced turbulence flow (Jahne et al., 1979), or bulk rms velocity at the interface is extrapolated from the liquid for the case of liquid-induced turbulence flow (see Khoo and Sonin, 1992). In fact, this was carried out in Law (2002) to facilitate the ease of reference to $K_L^+$ for the two types of turbulence generation, but it only further reinforces the (near) impossibility of finding a general relationship linking $K_L^+$ to the macroscale/bulk-based dimensionless grouping(s). One can easily foresee other difficulties arising if a turbulent flow is induced simultaneously from both above and below the liquid surface, as in a liquid flowing down a rough, inclined plane with a co/countercurrent flow of gaseous medium above.

## Concluding Summary

The improvement made in near-surface turbulent measurement, as in Law et al. (1999), has allowed the quantification of the vertical velocity with respect to the fluctuating interface and enables the evaluation of the associated velocity gradient at the interface ($\beta$). Hanratty and coworkers have shown that $\beta$ is an important hydrodynamic parameter controlling the scalar transport rate $(K_L)$ across the surface. In this work, $\beta$ was obtained for two vastly different near-surface turbulence conditions: one where turbulence is generated from beneath the interface; the other is wind-shear induced turbulence. Mass-transfer experiments were also carried out. It was found that a general correlation can be obtained relating the dimensionless $\beta$ $(\equiv \beta^+_{rms})$ to the scalar transport rate as

$$K_L^+ Sc^{0.5} = 0.22\, \beta^{+\ 0.5}_{rms}$$

which is applicable to the preceding turbulence conditions. Because $\beta^+_{rms}$ comprises hydrodynamics parameters measured/evaluated in a very small region that resides within a dimension much smaller than the turbulence macro-scale just

next to the interface, it is suggested that the present findings support the motion of universality of the small-eddy model used to account for the physics of interfacial mass transfer.

## Notation

$A$ = area of the interface
$C$ = concentration of the gas specimen in liquid
$C_i$ = initial concentration
$C_f$ = final concentration after time, $t$
$C_s$ = saturation concentration of the gas specimen in liquid
$d$ = nozzle diameter in the confined jet tank
$D$ = diffusivity of gaseous medium in the liquid
$D_t$ = tank diameter of the confined jet tank
$H$ = water depth in the wind–wave channel
$K_L$ = liquid-side mass-transfer velocity
$K_L^+$ = nondimensional liquid side mass-transfer rate ($\equiv K_L/\upsilon_{\beta\text{-}rms}$)
$l_s$ = small length scale
$Q$ = volumetric flow rate through the nozzle in the confined jet experiment
$Re_i$ = the interface Reynolds number ($\equiv(\upsilon_{i\text{-}rms}\Lambda_i)/\nu$)
$Re_s$ = system Reynolds number ($\equiv Q/d\nu$)
$Sc$ = Schmidt number ($\equiv \nu/D$)
$u$ = horizontal velocity component
$u^*$ = streamwise mean interfacial shear velocity based on liquid density
$U_{\text{mean}}$ = mean flow velocity in the direction of the wind
$\upsilon$ = vertical velocity component
$\upsilon_i$ = interface vertical velocity
$\upsilon_r$ = vertical velocity w.r.t the fluctuating interface
$\upsilon_\beta$ = velocity at which $\upsilon_r$ depart from the linear behavior
$Z_s$ = vertical location of the interface

### *Greek letters*

$\beta$ = vertical velocity gradient at the interface
$\beta_{rms}^+$ = nondimensional $\beta_{rms}$ ($\equiv \beta_{rms}\nu/\upsilon_{\beta\text{-}rms}^2$))
$\epsilon$ = rate of turbulence dissipation
$\lambda$ = eddy size
$\Lambda$ = macro length scale
$\Lambda_i$ = transverse integral length scale at the interface
$\bar{\Lambda}_{i/f}$ = distance from the interface where the variation of $\upsilon_{r\text{-}rms}$ is linear
$\nu$ = kinemetic viscosity
$\rho$ = density

### *Subscript*

*rms* = root-mean-square

## Literature Cited


Broecker, H., and W. Siems, "The Role of Bubbles for Gas Transfer from Water to Air at Higher Wind Speeds," *Gas Transfer at Water Surfaces*, W. Brutsaert and G. H. Jirka, eds., D. Reidel Publishing Company, Dordrecht, The Netherlands, 229 (1984).

Brignole, E. A., and R. Echarte, "Mass Transfer in Laminar Liquid Jets," *Chem. Eng. Sci.*, **36**, 695 (1981).

Brown, J. S., B. C. Khoo, and A. A. Sonin, "Rate Correlation for Condensation of Pure Vapour on Turbulent, Subcooled Liquid," *Int. J. Heat Mass Transfer*, **33**, 2001 (1990).

Campbell, J. A., and T. J. Hanratty, "Mass Transfer Between a Turbulent Fluid and a Solid Boundary: Linear Theory," *AIChE J.*, **29**, (2), 221 (1982).

Cheung, T. K., and R. L. Street, "Wave-Following Measurements in the Water Beneath an Air-Water Interface," *J. Geophy. Res.*, **93**, 14089 (1988).

Cox, J. D., and A. J. Head, "Solubility of Carbon Dioxide in Hydrofluoric Acid Solutions," *Trans. Faraday Soc.*, **58**, 1839 (1962).

Davidson, J. F., and E. J. Cullen, "The Determination of Diffusion Coefficients," *Trans. Inst. Chem. Eng.*, **35**, 51 (1957).

Duke, S. R., L. M. Wolff, and T. J. Hanratty, "Slopes of Small Scale Wind Waves and Their Relation to Mass Transfer Rates," *Exp. Fluids*, **19**, 280 (1995).

Fortescue, G. E., and J. R. A. Pearson, "On Gas Absorption into a Turbulent Liquid," *Chem. Eng. Sci.*, **22**, 1163 (1967).

George, J., F. Minel, and M. Grisenti, "Physical and Hydrodynamical Parameters Controlling Gas-Liquid Mass Transfer," *Int. J. Heat Mass Transfer*, **37**, 1569 (1994).

Gulliver, J. S., and A. Tamburrino, "Turbulent Surface Deformation and Their Relationship to Mass Transfer in an Open-Channel Flow," *Air-Water Gas Transfer*, B. Jahne, and E. C. Monahan, eds., Springer-Verlag, Delft, p. 589 (1995).

Hanratty, T. J., "Effect of Gas Flow on Physical Adsorption," *Air-Water Mass Transfer*, S. C. Wilhelm, and J. S. Gulliver, eds., American Society of Civil Engineers, Washington, DC, p. 10 (1990).

Hassan, Y. A., K. Okamoto, and O. G. Philip, "Investigation of the Interaction Between a Fluid Flow and the Fluid's Free Surface Using Particle Image Velocimetry," *Int. Symp. on Transport Phenomena in Thermal-Fluids Engineering* (ISTP-9), Pacific Center of Thermal Fluids Engineering, HI, 566 (1996).

Hering, F., C. Leue, D. Wierzimok, and B. Jahne, "Particle Tracking Velocimetry Beneath Water Waves. Part II: Water Waves," *Exp. Fluids*, **24**, 10 (1998).

Jahne, B., and H. Hau$\beta$ecker, "Air-Water Gas Exchange," *Annu. Rev. Fluid Mech.*, **30**, 443 (1998).

Jahne, B., K. O. Munnich, and U. Siegenthaler, "Measurements of Gas Exchange and Momentum Transfer in a Circular Wind-Water Tunnel," *Tellus*, **31**, 321 (1979).

Jahne, B., K. O. Munnich, B. Bosinger, A. Dutzi, W. Huber, and P. Libner, "On the Parameters Influencing Air-Water Gas Transfer," *J. Geophy. Res.*, **92**, (C2), 1937 (1987).

Khoo, B. C., and A. A. Sonin, "Scalar Rate Correlation at a Turbulent Liquid Free Surface: A Two-Regime Correlation for High Schmidt Numbers," *Int. J. Heat Mass Transfer*, **35**, 2233 (1992).

Khoo, B. C., T. C. Chew, P. S. Heng, and H. K. Kong, "Turbulence Characterisation of a Confined Jet Using PIV," *Exp. Fluids*, **13**, 350 (1992).

Khoo, B. C., Y. T. Chew, and C. J. Teo, "On Near-Wall Hot-Wire Measurements," *Exp. Fluids*, **29**, 448 (2000).

Komori, S., R. Nagaosa, and Y. Murakami, "Turbulence Structure and Mass Transfer Across a Sheared Air-Water Interface in Wind-Driven Turbulence," *J. Fluid Mech.*, **249**, 161 (1993).

Lamont, J. C., and D. S. Scott, "An Eddy Cell Model of Mass Transfer into the Surface of a Turbulent Liquid," *AIChE J.*, **16**, 513 (1970).

Law, C. N. S., B. C. Khoo, and T. C. Chew, "Turbulence Structure in the Immediate Vicinity of the Shear-Free Air-Water Interface Induced by a Deeply Submerged Jet," *Exp. Fluids*, **27**, 321 (1999).

Law, C. N. S., "Transport Across a Turbulent Air-Water Interface," PhD Diss., Dept. of Mechanical Engineering, National Univ. of Singapore (2002).

McCready, M. J., E. Vassihadou, and T. J. Hanratty, "Computer Simulation of Turbulent Mass Transfer at a Mobile Interface," *AIChE J.*, **32**, 1108 (1986).

Rashidi, M., and S. Banerjee, "Turbulence Structure in Free Surface Channel Flows," *Phys. Fluids*, **31**, 2491 (1988).

Rashidi, M., G. Hetsroni, and S. Banerjee, "Mechanism of Heat and Mass Transport at Gas-Liquid Interfaces," *J. Heat Mass Transfer*, **34**, 1799 (1991).

Saylor, J. R., and R. A. Handler, "Gas Transport Across an Air-Water Interface Populated with Capillary Waves," *Phys. Fluids*, **9**, 2529 (1997).

Sikar, K. K., and T. J. Hanratty, "Relation of Turbulent Mass Transfer to a Wall at High Schmidt Numbers to the Velocity Field," *J. Fluid Mech.*, **44**, 589 (1970).

Sonin, A. A., M. A. Shimko, and J. H. Chun, "Vapour Condensation onto a Turbulent Liquid-I. The Steady Condensation Rate as a Function of Liquid-Side Turbulence," *Int. J. Heat Mass Transfer*, **29** (9), 1319 (1986).

Theofanous, T. G., "Conceptual Models of Gas Exchange," *Gas Transfer at Water Surfaces*, W. Brutsaert and G. H. Jirka, eds., D. Reidel Publishing Company, Dordrecht, The Netherlands, p. 271 (1984).

Zhang, X., and C. S. Cox, "Measuring the Two-Dimensional Structure of a Wavy Surface Optically: A Surface Gradient Detector," *Exp. Fluids*, **17**, 225 (1994).


*Manuscript received June 1, 2001, and revision received Feb. 6, 2002.*